Structural and electrochemical characterization of lawsone-dependent production of tellurium-metal nanoprecipitates by photosynthetic cells of Rhodobacter capsulatus

Structural and electrochemical characterization of lawsone-dependent production of tellurium-metal nanoprecipitates by photosynthetic cells of *Rhodobacter capsulatus*

Roberto Borghese [a§*], Marco Malferrari[b*], Marco Brucale[c*], Luca Ortolani[d], Martina Franchini[a], Stefania Rapino[b], Francesca Borsetti[e], Davide Zannoni [a§]

[a]*Dept. of Pharmacy and Biotechnology FaBiT, University of Bologna, Bologna, Italy*

[b]*Dept. of Chemistry "Giacomo Ciamician", University of Bologna, Bologna, Italy*

[c]*Institute for the Study of Nanostructured Materials, CNR-ISMN, Bologna, Italy*

[d]*Institute for Microelectronics and Microsystems , CNR-IMM, Bologna, Italy*

[e]*Dept. of Biological, Geological and Environmental Sciences, University of Bologna, Bologna, Italy*

*****These authors contributed equally to this work

[§]Corresponding authors: Roberto Borghese roberto.borghese@unibo.it and Davide Zannoni

davide.zannoni@unibo.it

Abstract

Cells of the facultative photosynthetic bacterium *Rhodobacter (R.) capsulatus* exploit the simultaneous presence in the cultural medium of the toxic oxyanion tellurite (TeO_3^{2-}) and the redox mediator lawsone (2-hydroxy-1,4-naphthoquinone) by reducing tellurite to metal Te^0 nanoprecipitates (TeNPs) outside the cells. Here we have studied the mechanism by which lawsone interacts with metabolically active cells and analysed both structure and composition of the TeNPs collected from the growth medium of phototrophycally grown *R. capsulatus*. HR-TEM images and EDX microanalysis of TeNPs showed a central core of polycrystalline tellurium interspersed in an organic matrix with a predominant protein-based composition. The main proteins from Te^0 nanostructures were identified by Liquid Chromatography tandem-Mass Spectrometry and were all correlated with the cell outer membrane composition. The interaction of reduced lawsone with tellurite and with the bacterial cells was probed by Cyclic Voltammetry and Scanning ElectroChemical Microscopy (SECM). We concluded that lawsone is required for the reduction of tellurite to metal Te^0 in a reaction mechanism dependent on reducing equivalents deriving from the cell photosynthetic metabolism. SECM experiments demonstrate that lawsone, by diffusing inside the bacterial cells, is effectively available at the membrane site of the photosynthetic electron transport chain.

Keywords: lawsone; tellurite; tellurium nanoprecipitates; *Rhodobacter capsulatus*; Scanning ElectroChemical Microscopy (SECM)

1. Introduction

Tellurium (Te) is a metalloid that belongs to the Group 16 of the periodic table, and can exist in at least four redox states: telluride (Te^{-II}), metal tellurium (Te^{0}), tellurite (Te^{IV}) and tellurate (Te^{VI}). Prokaryotes and eukaryotes face tellurium mainly in the forms of oxyanions and organometalloids and some bacterial species can use tellurate (TeO_4^{2-}) and tellurite (TeO_3^{2-}) oxyanions as electron acceptors in the respiratory chain under anaerobic growth conditions [1,2]. In bacteria, TeO_3^{2-} reduction and precipitation in the form of metal Te^{0} takes place either in the cytoplasmic space, or externally to cells, e.g. on the cell surface and/or in the periplasmic space. Cytoplasmic tellurite reduction to crystal nanostructures of elemental Te^{0} has been described in several species such as *Rhodobacter sphaeroides* [3], *Rhodobacter capsulatus* [4], *Erythromicrobium ursincola* [5], the haloalkaliphilic archaeon *Natronococcus occultus* [6], *Pseudomonas pseudoalcaligenes* KF707 [7], Strain ER-Te-48 [1] and *Deinococcus radiodurans* [8], just to name a few, while exogenous Te^{0} deposits are mostly evident in those species, e.g. *Sulfurospirillum barnesii* and *Bacillus beveridgei*, able to use tellurite and tellurate as exogenous electron acceptors for anaerobic respiration [2].

Although chemical methods for the production of nanoparticles are extensively applied [9,10], even at large industry-ready scales [11], they typically involve the use of toxic reactants and organic solvents. This represents a curb both from an economic and from an environmental point of view, while also limiting their application in clinical fields. Microbiological methods to generate nanoparticles are regarded as safe, cost-effective and environment-friendly processes with a good scale-up potential for industrial production, but their development is presently a challenge. In this respect, it has been shown that quinone-type compounds can promote the reduction of Se^{IV} and Te^{IV} with the formation of extracellular nanoprecipitates [12]. An obvious advantage in the extracellular production of metal nanoparticles is the increase in yield and the reduction in costs of the isolation procedures. Further, in the case of particles accumulated on the external cell wall surface, the cells

themselves can be used as *in vivo* catalysts, e.g. *Shewanella oneidensis* MR-1 in the dechlorination of polychlorinated biphenyl (PCBs) by biopalladium particles [13].

Facultative phototrophic microorganisms of the genus *Rhodobacter* are highly amenable to biochemical and genetic manipulations [14], which make them ideal microbial systems for genetic engineering and molecular biology studies. We have recently reported that photosynthetic cells of *R. capsulatus* grown in a medium supplemented with lawsone (2-hydroxy-1,4-naphthoquinone), catalyze the extracellular accumulation of metal Te^0 nanoprecipitates (hereafter named: TeNPs) in contrast to the formation of intracellular deposits seen in the absence of lawsone [15,16]. Despite the interest in this observation, the knowledge gap in understanding the mechanism of bioformation of metal TeNPs precludes, at the present research stage, their production on a large scale using bacterial-based nano-manufacturing. Bacterial synthesis of TeNPs is generally achieved by a reduction step followed by a precipitation step with the latter composed of two parts: nucleation and crystal growth [17]. To date, only the biochemical mechanism, linked to the cytosolic reduction step of tellurite to metal tellurium, has been studied in some detail [14,18] whereas the bioprocesses responsible for tellurium nucleation and crystal growth are not fully understood, although there is some evidence that proteins might play a key role in growth of bacteriogenic metal TeNPs [19].

In the case of a lawsone dependent biosynthesis of exogenous TeNPs one may propose, as a working hypothesis, that a two steps mechanism is involved, namely: (i) the reduction of tellurite (TeO_3^{2-}) to elemental Te^0 mediated by the two electron carrier lawsone and (ii) the subsequent growth of Te^0 crystals into TeNPs possibly *via* the Ostwald ripening mechanism [16,18 ,20]. On the other hand, the process of TeNPs accretion might also include an alternative mechanism consisting of a lawsone mediated tellurite reduction in the periplasmic space and subsequent release into the growth medium of Te^0 crystals as outer membrane bulges through a process reminiscent of the cell vesicles generation [21]. Here, in an attempt to make the microbiological approach to the production of tellurium nanostructures less empirical, the structural features of exogenously

generated TeNPs by photosynthetic cells of *R. capsulatus* were investigated by a combination of chemical (SDS-PAGE, LC-MS/MS, Voltammetry) and physical techniques [TEM, energy dispersive X-ray (EDX), Dynamic Light Scattering (DLS)]. These approaches have shown the inner crystalline tellurium structure of the TeNPs and identified a number of proteins forming an external organic coating which are also components of the outer membrane of the bacterial cell. Electrochemical techniques and scanning electrochemical microscopy, in particular, were already employed to deeply characterize cells, nanomaterials and their interactions with biological species and to elucidate redox mediated biological processes [22-26].

In this work, the electrochemical investigation demonstrated that lawsone is indeed capable to diffuse into the bacterial cell membrane and may mediate the shuttling of reducing equivalents (electrons) from the membrane-bound photosynthetic apparatus to soluble tellurite molecules which precipitate as metal TeNPs. To our knowledge, this is the first time that the electrochemical features of lawsone and tellurite were examined together in a chemical solution and in the presence of metabolically active cells.

2. Experimental

2.1. Growth conditions and tellurium nanoprecipitates preparation

Rhodobacter capsulatus strains B100 (wild type) and bKSDF mutant (Δ*fla*A, no flagellum) [27] were grown in RCV minimal medium [28] under anaerobic photosynthetic conditions with 30 mM pyruvate as the sole carbon source. Cells suspensions were then diluted 1:10 in a filled screw-capped tubes containing fresh growth medium, with the same carbon source of the starting culture, and anaerobiosis was obtained upon incubation for 20 hrs in the dark, to allow for the complete O_2 consumption by cell respiration [29]. After reaching anaerobiosis, K_2TeO_3 and lawsone were each added at a concentration specified for the single experiments in the Results section, and the tubes, kept at 30°C in a thermostated water bath, were illuminated by incandescent light lamps (200

W/m^2). TeNPs were prepared after incubation of the microbial cultures in the light for 24 hrs. The cultures were centrifuged at 27,200 x g for 15 min to harvest the cells. The obtained supernatant was centrifuged in a Beckman L-90K ultracentrifuge at 109,000 x g for 30 min and the collected nanoprecipitates were washed once in Milllipore purified water.

2.2. TEM microscopy

TeNPs were characterized using Transmission Electron Microscopy (TEM) FEI Tecnai F20 ST, equipped with CCD Camera Gatan MSC704 and X-Rays EDS spectrometer EDAX EDS PV9761. TEM samples were prepared by drop casting the nanoprecipitates solutions onto a standard TEM holey carbon grid, wicked with filter paper to remove excess solution and dried in air for 20 min.

2.3. Dynamic Light Scattering and ζ-potential measurements

DLS and zeta potential (ζ) measurements were performed on a NanoBrook ZetaPALS (Brookhaven Instruments Corporation, USA) equipped with a BI-870 Dielectric Constant Meter. Aliquots from purified TeNPs suspensions were pelleted by centrifugation at 10k for 30 min and then suspended in one of the following solutions: 100 mM citrate (buffered at pH values of 2.60, 2.80, 3.25, 3.50, 4.00, 4.25, 5.00), 100 mM phosphate (buffered at pH 6.15, 6.60, 7.20, 7.85, 8.25), 100 mM borate buffer (pH 8.00, 8.33, 9.00, 9.33, 10.00, 10.33, 10.66). All DLS (effective diameter) and phase analysis light scattering (ζ) measurements were performed in triplicate on the same preparations.

2.4. SDS-PAGE and Sample preparation for LC-MS/MS analysis

TeNPs suspensions were pelleted and suspended in 50µl of Reb2 Buffer (20 mM Tris buffer-pH 6.8, 7M Urea, 2M Thiourea, 4% w/v CHAPS, 50 mM DTT) and incubated with continuous shaking at room temperature for 30 min. After incubation the samples were centrifuged for 15 min in a minifuge at maximum speed and the supernatants, with the solubilized proteins, were stored at -80°C. All reagents were purchased from Millipore-Sigma (St. Louis, USA).

For SDS-PAGE 30 µl of each sample were thawed, diluted in the reducing Laemmly buffer [30], and run on a 12% SDS-polyacrylamide gel in Tris-Glycine buffer under constant current (0.02 A, 250 V max) in Miniprotean TetraCell (BioRad, Hercules, USA). The gel was then fixed for 2 hours in fixing solution (Methanol 40%, Acetic Acid solution 10%), stained O/N with 0.1% Colloidal Coomassie and scanned with Pharos-FX system (BioRad, Hercules, USA).

Protein bands indicated as A, B, C and D were excided from the gel and treated as reported by Shevchenko et al. [31]. Briefly, spots were destained in 50 mM ammonium bicarbonate in acetonitrile (ACN) and dehydrated with pure ACN. Samples were then reduced with 10 mM DTT and alkylated with 55 mM iodoacetamide in 100 mM ammonium bicarbonate (Millipore-Sigma, St. Louis, USA). After dehydration in ACN, gel pieces were equilibrated at 4 °C in solution A (10 mM ammonium bicarbonate, 10 % ACN) containing 13 ng/µl of porcine trypsin for MS (Millipore-Sigma) for 2 hrs, and then incubated at 37 °C overnight. After spinning, supernatants were harvested and gel pieces were covered by extraction solution (5 % formic acid in ACN). After 15 minutes of incubation at 37 °C, supernatants from this step where pooled to the corresponding supernatants of the previous step and dried in SpeedVac (SavantTM).

2.5. Mass spectrometry analysis

LC-MS/MS (Liquid Chromatography tandem-Mass Spectromerty) analysis on the trypsin digested proteins was performed at C.I.G.S. (Centro Interdipartimentale Grandi Strumenti), University of Modena and Reggio Emilia, as follows. Dry peptides from fractions were suspended in 25 µl of a mixture of water: acetonitrile: formic acid 97:3:2, sonicated for 10 min at room temperature and centrifuged at 12,100 r.c.f. for 10 min. Analyses were performed on an ESI-Q-TOF Accurate-Mass spectrometer (G6520A, Agilent Technologies, Santa Clara, CA, USA), controlled by MassHunter software (v. B.04.00) and interfaced with a CHIP-cube to an Agilent 1200 nano-pump. Two biological replicates were performed for each sample. Chromatographic separation was performed

on a chip (Agilent Technologies) with a 75 µm I.D., 43 mm, 300 Å C18 column, prior to a desalting step through a 40 nl trap column.

2.6. Protein identification

Raw data, converted from the vendor's data format into mascot generic format using MassHunter Qualitative Analysis (v. B.05.00), were searched against Swiss-Prot (v. 2013_06, 550740 entries for Homo Sapiens) and for peptide sequences and C-RAP (ftp://ftp.thegpm.org/fasta/cRAP, 116 entries) for contaminants with MASCOT (Version 2.4, Matrix Science, London, UK). The following search parameters were used: 40 ppm precursor tolerance, 0.05 Da fragment mass error allowed, two missed cleavage allowed for trypsin, carbamidomethyl as a fixed modifier of cysteine residues and methionine oxidation, deamidated NQ, Gln->pyro-Glu N-term Q, Glu->pyro-Glu N-term E as variable modifications. The false discovery rate was estimated through an internal decoy database search; all results were filtered in order to have a FDR < 0.1.

2.7. Electrochemical measurements

Electrochemical measurements were performed in a teflon electrochemical cell with a three electrodes set up controlled by a CHI910B SECM bipotentiostat from CH Instruments Inc. (Austin, Texas). A platinum wire was employed as counter electrode, an Ag/AgCl (KCl 3 M) (CH Instruments Inc., product number CHI111) as reference electrode and glassy carbon of 1 mm diameter (SGCE Glassy carbon electrode, product number 002412, ALS Co., Ltd. Tokyo, Japan) as working electrode. Cyclic voltammetry (CV) of 5 mM lawsone (Figure 4A) is representative of three independent measures performed at 0.02 V/s, in PBS buffer and RCV medium. CV of 25 µM lawsone showed in Figure S2C is representative of four independent measurements performed at scan rates ranging from 0.02 to 0.16 V/s in PBS buffer and RCV medium. CVs of Figure 4B are representative of three independent measures performed on 10 mM potassium tellurite in PBS, in a potential window of -0.8 - 0.5 V vs Ag/AgCl (3 M KCl); five independent measurements were

performed for 1 mM potassium tellurite in PBS, at several scan rates in the range of 0.02 to 0.16 V/s. CVs of 1 mM potassium tellurite in the presence of 25 μM lawsone (Figure 5) are representative of four independent measurements at scan rate 0.02 V/s. Figure 7 shows four SECM approach curves both in the presence and in the absence of bacteria attached to the approached surface.

For the real time measurement of tellurite reduction by photosynthetic bacterial culture under anoxic conditions, anaerobic conditions were obtained by continuously fluxing argon in the culturing medium, while constant temperature of 30°C were obtained by immersing the culture/electrochemical cell in a water bath at 30°C.

For SECM approach curves, bacterial cells were adsorbed to the glassy bottom of a 3.5 cm diameter petri dish; the glass surface was incubated for 5 minutes with D-polylisine (Merck Millipore, product code A-003-E) and then washed with sterile double distilled water. Bacterial cell suspension was then incubated at room temperature for approximately 2 hrs in a petri dish containing the polylisine-modified surface. At the end, not adhering cells were removed by washing with sterile PBS buffer. SECM approaches were performed on these samples in the presence of 200 μM lawsone in PBS buffer under aerobic conditions. A 10 μm Pt ultamicroelectrode was employed (RG=10) as SECM probe, a Pt wire was used as counter electrode and an Ag/AgCl (3M/KCl) served as reference electrode. The applied potential was E= -0.5 V vs Ag/AgCl (3M KCl).

3. Results and Discussion

3.1. Morphology, composition and crystallinity

The nanoscale morphological characterization of purified TeNPs was performed via transmission electron microscopy. Lower magnification TEM images (Fig. 1A) showed elongated needle-like nanoprecipitates with an average diameter of 10 ± 5 nm and an axis: diameter aspect ratio of around 20:1. High-resolution electron microscopy (HREM) images (Fig. 1B), and Fast Fourier Transform (FFT) analysis of those images (Fig. 1C) shows that the needles are constituted by Te^0 crystals, with the axis of the needle oriented along the (100) crystallographic direction. Individual nanostructures

were rarely observed, since most were found either in bundles of 2-6 laterally adjoining parallel needles, or in roughly star-shaped clusters of 2-4 bundles radiating from a central core. Fig. 1D shows a HREM image of the central core, made of polycrystalline Te, providing a growth origin for the individual needles oriented along the (100) direction of each grain. The relative FFT analysis (Fig. 1E) shows the characteristic reflections from Te crystals, identified as the (110), (011) and (100) family of planes, spaced, respectively, 0.22 nm, 0.32 nm and 0.39 nm. EDX microanalysis was performed over one of those bundles, showing the peaks corresponding to Te along with weaker peaks from the residues of the organic content of the solutions, as P, S and Cl traces (Fig. 1F). From the HREM images collected, it is possible to see the presence of an amorphous thin coverage (1-2 nm) all over the needles, probably made of organic molecules form the growth mediated by micro-organisms (see below).

3.2. Zeta (ζ) potential and dynamic light scattering

In an attempt to further investigate the colloidal properties of TeNPs and their surface coating, we performed a series of zeta-potential (ζ) and effective hydrodynamic radius (R_H) measurements at various pH values ranging from highly acidic to strongly basic (~2.5-11.5). Due to the impossibility of using the same buffer solution across such a large pH interval, we subdivided it into three ranges (see Materials and Methods for details). Purified TeNPs from three distinct production batches were divided into aliquots which were resuspended at various pH values; on each aliquot, we measured R_H (via DLS) and ζ (via phase analysis light scattering). Results are plotted in Fig. 2 and Fig. S1. As a preliminary remark to the interpretation of these results, it is important to note that we did not base any of our conclusions on absolute R_H and ζ and values. This is due to several reasons, namely: a) the measured values vary considerably between production batches, probably because of an intrinsic variance in purification/synthesis procedures resulting in slightly different compositions, ionic strengths and particle length and size; b) individual ions in different buffer solutions could interact differently with the TeNP surface, resulting in artifacts; and c) TeNPs have a needle-like

morphology with high (and highly dispersed) aspect ratio, making R_H values only meaningful on a broadly qualitative basis. Despite these limitations, it is possible to draw some conclusions on the R_H and ζ data.

All the measured ζ values are negative at all pH values, ranging between -2 and -25 mV. These absolute values are generally considered too low to provide lasting stability to colloidal dispersions; but even TeNPs solutions from production batches resulting in very low ζ values (e.g. the batch identified by squares in Fig. 2) was stable for several days. This suggests that the main factor hindering TeNPs aggregation and contributing to TeNPs stability is not electrostatic repulsion, but steric shielding provided by some sort of negatively charged coating, possibly constituted by scarcely self-interacting organic material [32].

We observed no significant changes to either R_H or ζ across the entire range, except for one sharp ζ transition to less negative values occurring below pH ~3.5 in all measured batches (Fig. 2, lower panel). It is important to note that the same samples showed no concurrent transition in R_H at the same pH (Fig. 2, top panel). Fitting the ζ values from each batch with a Boltzmann sigmoid yields an average transition pH value of 3.45 ± 0.05. To check whether the induced transition was reversible, we pelleted, washed and suspended all aliquots from a previously measured batch at pH 3.0, noting that all of them converged at roughly the same ζ value (Fig. S1-b, circles). Then, the same aliquots were pelleted, washed and suspended at different pH values, returning to ζ values similar to those originally measured prior to resuspension at pH 3.0 (Fig. S1b, crosses). This demonstrates that the induced ζ transition is due to a fully reversible process occurring around pH 3.5. Taken together, these observations are compatible with the hypothesis that the sharp ζ transition might be due to the reversible protonation of groups with a pK_a around 3.5 on the organic TeNPs coating, e.g. carboxyl, hydroxyl or imidazol moieties.

3.3. Determination of the proteins on the TeNPs organic coating

The pK_a at pH 3.5, determined by ζ-potentials, and the presence of amide and carboxylic groups, evidenced by FT-IR analysis [16], are strongly indicative of a TeNPs' organic coating that contains proteins as a fundamental component. To conclusively establish the presence of polypeptides on *R. capsulatus'* TeNPs, and to identify which proteins, if any, are specifically associated to the nanoprecipitates, an SDS-PAGE was run with proteins solubilized from particles prepared under different growth conditions (Fig. 3). Proteins solubilized from TeNPs produced by wild type B100 cells are shown in lane 1. A 40 kD major band (A in Fig. 3) was identified, by LC-MS/MS, as flagellin and was also found in cells grown without tellurite that did not produce TeNPs (Fig. 3, lane 3). As a control, proteins extracted from TeNPs produced by the Fla^- mutant bKSDF, which does not synthesize flagellin, totally lacked the 40 kD band, as expected, while still retaining the ability to produce normal TeNPs (Fig. 3, lane 5). Three other bands, identified as B, C and D, were either absent or present at a lesser intensity in the tellurite-less sample, with no TeNPs produced, as compared with all the other samples from cells grown in the presence of tellurite and that produced nanoprecipitates. LC-MS/MS analysis led to the identification of the protein associated to the three bands. Band B, totally absent in preparations from cultures not producing TeNPs (Fig. 3, lane 3), consisted of two proteins identified as a Peptidase of the M10 family (MW 61 kD) and a TonB-dependent receptor (MW 66 kD). Band D, also found only in preparations from TeNPs producing cells (Fig. 3, lanes 1, 2, 4, 5), comprised two main proteins, a Porin (MW 32 kD) and a putative Lipoprotein (MW 32 kD). Band C was analyzed because, despite being present in all preparations, it was, apparently, much less abundant in the absence of tellurite. One protein was identified as a large protein involved in heme utilization (MW 90 kD). Interestingly, all these polypeptides were found to be highly homologous to proteins associated to the outer membrane in Gram negative bacteria. This suggests that, during nanoprecipitates formation, outer membrane fragments may bleb off and associate with the particles. Whether any of these proteins have an active role in the assembly of the TeNPs remains to be determined.

3.4. Electrochemical analysis of lawsone and tellurite

Electrochemical behaviour of lawsone and potassium tellurite in phosphated-saline buffer (PBS) at pH 7.4 in anoxic conditions was investigated by cyclic voltammetry (CV) in the range -0.8 ÷ 0.5 V vs Ag/AgCl (KCl 3 M); representative measurements are reported in Fig. 4 (see Experimental section for more details). Lawsone shows two reduction peaks; a first reduction peak at $E_{1/2}$ = -(0.360 ± 0.005) V and a second reduction peak at – (0.62 ± 0.005) V vs Ag/AgCl (3 M KCl), corresponding to $E_{1/2,1}$ = -0.15 V and $E_{1/2,2}$ = -0.41 V vs normal hydrogen electrode. Potassium tellurite shows two irreversible peaks at reducing and oxidative potentials: a reduction peak at around -0.6 V and an oxidation peak at 0.1 V vs Ag/AgCl (3 M KCl), respectively. Lawsone CVs show features of a free diffusing analyte that is oxidized/reduced at the working electrode [33,34], tellurite CVs shapes suggest the occurrence of adsorption/desorption phenomena of the species at the surface of the working electrode during reducing/oxidizing cycles. To better elucidate the aforementioned phenomena, potassium tellurite CVs in PBS were additionally investigated by changing progressively the lower vertex potential values to -0.1, -0.4, -0.6 and -0.8 V, as reported in panel A of Fig. S2. An oxidation peak (E > 0.1 V) is observed only cycling at reducing potential lower than -0.6 V.

Potassium tellurite and lawsone in bacterial culture are used at lower concentrations than the ones explored in the CVs reported in Fig. 4, therefore voltammetries of 1 mM potassium tellurite and 25 μM lawsone in PBS were recorded to study their electrochemical behaviour at bacterial operating concentrations. No relevant differences are observed at these concentrations for potassium tellurite (Fig. S2, panel B), while lawsone at a concentration of 25 μM in PBS shows only one of the two reduction peaks, at - (0.415 ± 0.005) V vs Ag/AgCl (3 M KCl) (Fig. S2, panel C). Likely, at this concentration, the residual oxygen in solution is sufficient to react with the mono-reduced form of lawsone preventing the formation of its double reduced form.

A solution of 1 mM potassium tellurite and 25 μM lawsone in RCV medium was investigated by CV in anoxic conditions. When comparing CVs of 1 mM potassium tellurite in PBS and in RCV medium (Fig. S3), a relevant increase of tellurite current peak intensities is observed, together with a shift of tellurite reduction peak to lower potentials, from - (0.380 ± 0.005) V to - (0.460 ± 0.005) V vs Ag/AgCl (3 M KCl). Additionally, the peaks of tellurite reduction move towards less reducing potentials (of approximately +30 mV in the first two cycles), indicating that when lawsone is present tellurite reduction is facilitated.

Cyclic voltammetries of potassium tellurite performed in absence and in presence of lawsone in RCV medium (Fig. 5) show that a redox interaction between reduced lawsone and oxidized tellurite takes place in bacterial culturing conditions. The reduction current of tellurite increases in presence of lawsone, indicating that lawsone catalyses the tellurite reduction (Fig. 5, inset). Additionally, peaks of tellurite reduction move towards less reducing potentials (of approximately +30 mV in the first two cycles), indicating that when lawsone is present tellurite reduction is facilitated. The potential at which tellurite peak increases in the presence of lawsone corresponds to the reduction potential of lawsone $E_{m,1}$ = -0.36 V vs Ag/AgCl; the amount of current increase cannot be ascribed to the lawsone reduction by itself. These results suggest that tellurite reduction is mediated by lawsone.

We performed cyclic voltammetries on cell cultures grown under illumination in the presence of tellurite and lawsone. With these measurements, we investigated if tellurite is reduced by *R. capsulatus* cells redox activity via lawsone mediation: reduced tellurite by the photosynthetic cells was detected at 0.1 V vs Ag/AgCl by cycling the potential between -0.1 and 0.5 V. In this potential range, an oxidation current is detected only if tellurite is previously reduced by the cell's metabolic activity. Furthermore, the oxidation current value is related to the amount of reduced tellurite present in the medium. As showed in panel A of Fig. 6, when light is turned on an increase of the current of tellurite oxidation peak at approximately 0.1 V, is observed. The quantification of peak

heights at 0.1 V resulted in the kinetics of reduced tellurite formation in culturing conditions (Fig. 6B), most probably as a consequence of bacterial photosynthetic processes.

In view of this latter result, we investigated the cell membrane permeability to lawsone. SECM approach curves in the presence of 200 μM lawsone (serving as the redox species in feedback mode) were performed on a layer of bacteria attached through polylysine to the glass bottom of a Petri dish. As schematized in Fig. S4, SECM approach curves give us information on the permeability of the approached surface to the compound reduced/oxidized at the probe [35]; in our case, the reduction of lawsone is measured at the probe biased at -0.5 V vs Ag/AgCl. As reported in Fig. 7, in the absence of bacteria, SECM approach curves (black empty symbols) are highly reproducible and can be fitted with a model that describes an insulating surface not permeable to lawsone (grey traces) [36,37]. In the presence of a layer of bacteria attached to the surface of the Petri dish with polylysine (Fig. S4, panel C), SECM approach curves (Fig. 7, empty red symbols) are poorly fitted with the insulating model. On the contrary, the approach curves in the presence of bacteria can be accurately fitted with a model that considers a certain permeability of the surface to lawsone (see Supporting information for more details). Our conclusion is also supported by electrochemical experimental evidence combined to density functional theory calculations, indicating that the limiting electron transfer step between monomeric quinone mediators and the active sites takes place in the liphophilic membrane of *R. capsulatus* cells [38].

SECM approach curves on deposited *R. sphaeroides* cells in the presence of several redox mediators have been reported in the literature [39]. The analysis of our approach curves resulted in permeability values (Table 1 of Supporting information) that are in good agreement with those reported by Cai and colleagues regarding *R. sphaeroides* permeability to 1,4-naphtoquinone and 1,2-naphtoquinone.

These results demonstrate that lawsone diffuse inside bacterial cells supporting the concept that lawsone is effectively available at the site of anoxygenic photosynthesis to receive electrons (as proposed in [15]) and to pass them to tellurite.

4. Conclusions

HREM and EDX analyses showed that the tellurium nanoprecipitates made by photosynthetically growing *R. capsulatus* cells are composed of a central core of polycrystalline Te interspersed in an organic matrix. Zeta-potential measurements indicated that on the surface of the TeNPs are present chemical groups with a pK_a around 3.5, indicative of carboxyl and, possibly, imidazole groups. Proteins solubilized from the nanostructures were identified by LC-MS/MS and were all recognized as associated to the bacterial outer membrane.

Electrochemical analyses revealed that lawsone diffuses inside the bacterial cells and that during growth a redox interaction takes place between reduced lawsone and tellurite. This process depends on the photosynthetic metabolism which supplies the reducing equivalents deriving from pyruvate as the sole carbon source.

Acknowledgements

We acknowledge the SPM@ISMN facility for AFM measurements and data analysis support. DZ, RB and SR were supported by University of Bologna (RFO grants 2016-2017).

References

[1] J.T. Csotonyi, E. Stackebrandt, V, Yurkov, Anaerobic respiration on tellurate and other metalloids in bacteria from hydrothermal vent fields in the eastern Pacific Ocean, Appl. Environ. Microbiol. 72 (2006) 4950-4956.

[2] S.M. Baesman, T.D. Bullen, J. Dewald, D.H. Zhang, S. Curran, F.S. Islam, T.J. Beveridge, R.S. Oremland, Formation of tellurium nanocrystals during anaerobic growth of bacteria that use Te oxyanions as respiratory electron acceptors, Appl. Environ. Microbiol. 73 (2007) 2135-2143.

[3] M.D. Moore, S. Kaplan, Members of the family *Rhodospirillaceae* reduce heavy-metal oxyanions to maintain redox poise during photosynthetic growth, ASM News 60 (1994) 17–24.

[4] F. Borsetti, R. Borghese, F. Francia, M.R. Randi, S. Fedi, D. Zannoni, Reduction of potassium tellurite to elemental tellurium and its effect on the plasma membrane redox components of the facultative phototroph *Rhodobacter capsulatus*, Protoplasma 221 (2003) 152-161.

[5] V. Yurkov, J. Jappé, A. Verméglio, Tellurite resistance and reduction by obligately aerobic photosynthetic bacteria, Appl. Environ. Microbiol. 62 (1996) 4195-4198.

[6] C.T. Pearion, P.E. Jablonski, High level, intrinsic resistance of *Natronococcus occultus* to potassium tellurite, FEMS Microbiol. Lett. 174 (1999) 19-23.

[7] G. Di Tomaso, S. Fedi, M. Carnevali, M. Manegatti, C. Taddei, D. Zannoni, The membrane-bound respiratory chain of *Pseudomonas pseudoalcaligenes* KF707 cells grown in the presence or absence of potassium tellurite, Microbiology 148 (2002) 1699-1708.

[8] N. Anaganti, B. Basu, A. Gupta, D. Joseph, S.K. Apte, Depletion of reduction potential and key energy generation metabolic enzymes underlies tellurite toxicity in *Deinococcus radiodurans*, Proteomics 15 (2015) 89-97.

[9] F. Beshkari, S. Zinatloo-Ajabshir, M. Salavati-Niasari, Preparation and characterization of the $CuCr_2O_4$ nanostructures via a new simple route, J. Mater. Sci: Mater. Electron. 26 (2015) 5043-5051.

[10] S. Zinatloo-Ajabshir, M. Salavati-Niasari, Preparation and characterization of nanocrystalline praseodymium oxide via a simple precipitation approach, J. Mater. Sci: Mater. Electron. 26 (2015) 5812-5821.

[11] C.A. Charitidis, P. Georgiou, M.A. Koklioti, A-F. Trompeta, V. Markakis, Manufacturing nanomaterials: from research to industry, Manufacturing Rev. 1 (2014) 11.

[12] X. Wang, G. Liu, J. Zhou, J. Wang, R. Jin, H. Lv, Quinone-mediated reduction of selenite and tellurite by *Escherichia coli*, Bioresour. Technol. 102 (2011) 3268-3271.

[13] D. De Windt, P. Aelterman, W. Verstraete, Bioreductive deposition of palladium (0) nanoparticles on *Shewanella oneidensis* with catalytic activity toward reductive of dechlorination of polychlorinated biphenyls, Environ. Microbiol. 7 (2005) 314-325.

[14] D. Zannoni, F. Borsetti, J.J. Harrison, R.J. Turner, The bacterial response to the chalcogen metalloids Se and Te, Adv. Microb. Physiol. 53 (2008) 1-71.

[15] R. Borghese, C. Baccolini, F. Francia, P. Sabatino, R.J. Turner, D. Zannoni, Reduction of Chalcogen Oxyanions and Generation of Nanoparticles by the Photosynthetic Bacterium *Rhodobacter capsulatus*, J. Hazard. Materials 269 (2014) 24-30.

[16] R. Borghese, M. Brucale, G. Fortunato, M. Lanzi, A. Mezzi, F. Valle, M. Cavallini, D. Zannoni, Extracellular production of tellurium nanoparticles by the photosynthetic bacterium *Rhodobacter capsulatus*, J. Hazar. Materials 309 (2016) 202-209.

[17] C.I. Pearce, V.S. Coker, J.M. Charnock, R.A.D. Pattrick, J.F.W. Mosselmans, N. Law, T.J. Beveridge, J.R. Lloyd, Microbial manufacture of chalcogenide-based nanoparticles via the reduction of selenite using *Veillonella atypica*: an in situ EXAFS study, Nanotechnology 19 (2008) 155603.

[18] R.J. Turner, R. Borghese, D. Zannoni, Microbial processing of tellurium as a tool in biotechnology, Biotechnol. Adv. 30 (2012) 954-963.

[19] R. Jain, N. Jordan, S. Weiss, H. Foerstendorf, K. Heim, R. Kacker, R. Hübner, H. Kramer, E.D. van Hullebusch, F. Farges, P.N.L. Lens, Extracellular polymeric substances govern the surface charge of biogenic elemental selenium nanoparticles, Environ. Sci. Technol. 49 (2015) 1713-1720.

[20] W. Zhang, Z. Chen, H. Liu, L. Zhang, P. Gao, D. Li, Biosynthesis and structural characteristics of selenium nanoparticles by *Pseudomonas alcaliphila*, Colloid. Surface B 88 (2011) 196-201.

[21] B. György, T.G. Szabó, M. Pásztói, Z. Pál, P. Misják, B. Aradi, V. László, É. Pállinger, E. Pap, Á. Kittel, G. Nagy, A. Falus, E.I. Buzás, Membrane vesicles, current state-of-the-art: emerging role of extracellular vesicles, Cell. Mol. Life Sci. 68 (2011) 2667-2688.

[22] S. Rapino, E. Treossi, V. Palermo, M. Marcaccio, F. Paolucci, F. Zerbetto, Playing peekaboo with graphene oxide: a scanning electrochemical microscopy investigation, Chem. Comm. 50 (2014) 13117.

[23] S. Rapino, R. Marcu, A. Bigi, A. Soldà, M. Marcaccio, F. Paolucci, P.G. Pelicci, M. Giorgio, Scanning electro-chemical microscopy reveals cancer cell redox state, Electrochim. Acta 179 (2015) 65-73.

[24] A. Soldà, G. Valenti, M. Marcaccio, M. Giorgio, P.G. Pelicci, F. Paolucci, S. Rapino, Glucose and Lactate Miniaturized Biosensors for SECM-Based High-Spatial Resolution Analysis: A Comparative Study, ACS Sens. 2 (2017) 1310-1318.

[25] L. Bartolini, M. Malferrari, F. Lugli, F. Zerbetto, F. Paolucci, P.G. Pelicci, C. Albonetti, S. Rapino, Interaction of Single Cells with 2D Organic Monolayers: A Scanning Electrochemical Microscopy Study, ChemElectroChem 5 (2018) 1-8.

[26] T-E. Lin, S. Rapino, H.H. Girault, A. Lesch, Electrochemical imaging of cells and tissues, Chem. Sci. 9 (2018) 4546.

[27] K.J. Shelswell, J.T. Beatty, Coordinated, long-range, solid substrate movement of the purple photosynthetic bacterium *Rhodobacter capsulatus*, PLoS ONE 6 (2011) e19646.

[28] P.F. Weaver, J.D. Wall, H. Gest, Characterization of *Rhodopseudomonas capsulate*, Arch. Microbiol. 105 (1975) 207-216.

[29] R. Borghese, F. Borsetti, P. Foladori, G. Ziglio, D. Zannoni, Effects of the metalloid oxyanion tellurite (TeO_3^{2-}) on growth characteristics of the phototrophic bacterium *Rhodobacter capsulatus*, Appl. Environ. Microbiol. 70 (2004) 6595-6602.

[30] U.K. Laemmly, Cleavage of structural proteins during assembly of the head of bacteriophage T4, Nature 227 (1970) 680-685.

[31] A. Shevchenko, H. Tomas, J. Havliš, J.V. Olsen, M. Mann, In-gel digestion for mass spectrometric characterization of proteins and proteomes, Nat. Protoc. 1 (2006) 2856-2860.

[32] E. Piacenza, A. Presentato, R.J. Turner, Stability of biogenic metal(loid) nanomaterial related to the colloidal stabilization theory of chemical nanostructures, Critical Reviews Biotechnology 38 (2018) 1137-1156.

[33] J.S. Bard, L.R. Faulkner, Electrochemical Methods – Fundamentals and Applications, 2nd ed., John Wiley and Sons, 2001.

[34] N. Elgrishi, K.J. Rountree, B.D. McCarthy, E.S. Rountree, T.T. Eisenhart, J.L. Dempsey, A practical beginner's guide to cyclic voltammetry, J. Chem. Educ. 95 (2018) 197-206.

[35] J.A. Bard, M.V. Mirkin, Scanning Electrochemical Microscopy, 2nd ed., CRC Press, Taylor and Francis Group, 2012.

[36] R. Cornut, C. Lefrou, A unified new analytical approximation for negative feedback currents with a microdisk SECM tip, J. Electroanal. Chem. 608 (2007) 59-66.

[37] R. Cornut, C. Lefrou, New analytical approximation of feedback approach curves with a microdisk SECM tip and irreversible kinetic reaction at the substrate, J. Electroanal. Chem. 621 (2008) 178-184.

[38] M. Grattieri, Z. Rhodes, D.P. Hickey, K. Beaver, S.D. Minteer, Understanding biophotocurrent generation in photosynthetic purple bacteria, ACS Catalysis 9 (2019) 867-873

[39] C, Cai, B. Liu, M.V. Mirkin, Scanning Electrochemical Microscopy of Living Cells. 3. *Rhodobacter sphaeroides*, Anal. Chem. 74 (2002) 114-119.

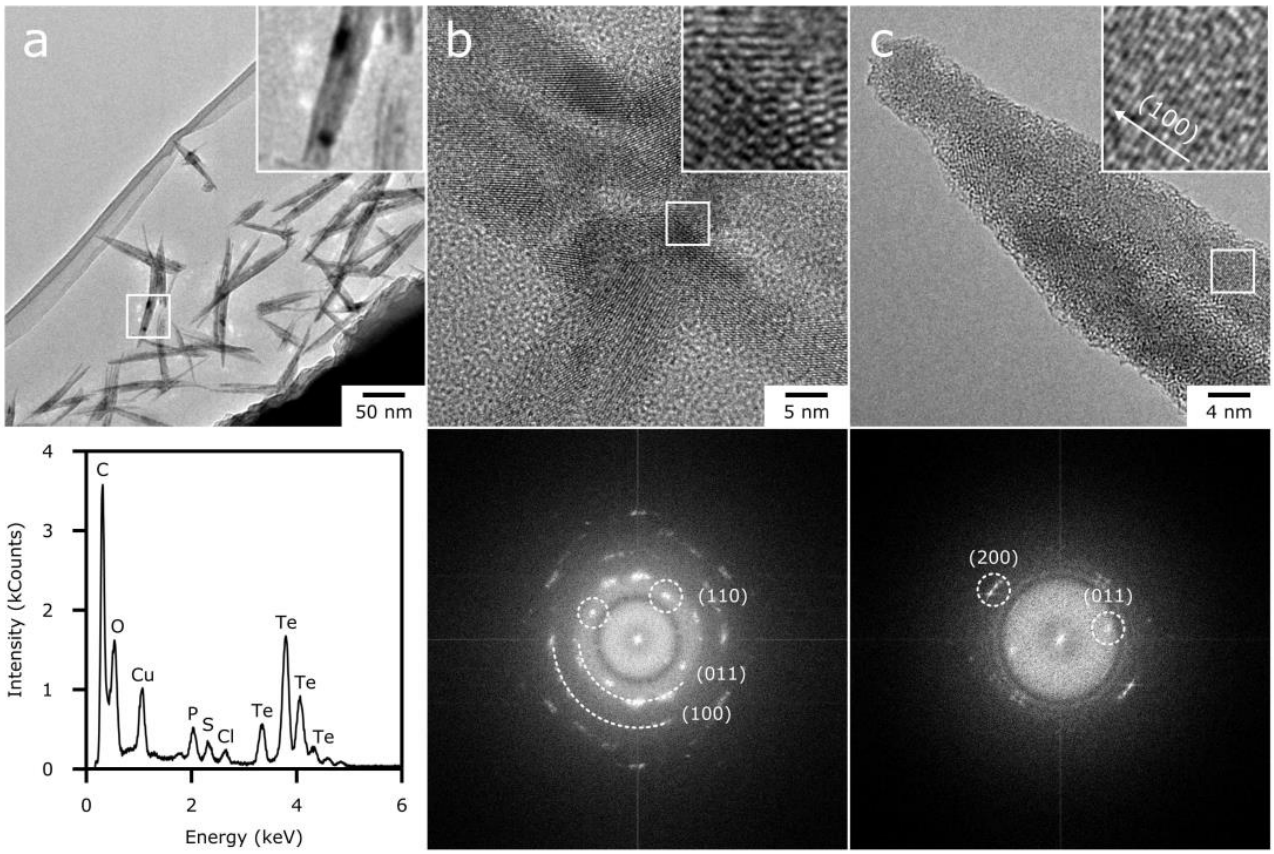

Figure 1. TEM analysis. (A) TEM micrograph of the nanostructures bundles lying over the carbon film of the TEM grid. (B) HREM image of the tip of one of the needles, showing lattice fringes from (100) Te crystal (inset), oriented along the axis of the nanostructure. (C) FFT of the image in (B) showing reflections from (200) and (011) planes of Te crystal. (D) HREM detail of the central core of the needles, showing the interconnected growth of the TeNPs. Inset shows a 4x detail of the lattice fringes in region outlined. (E) FFT of the image in (D) showing reflections identified as from the (110), (011) and (100) family of planes in Te crystals, spaced, respectively, 0.22 nm, 0.32 nm and 0.39 nm. (F) EDX spectrum showing the composition of the region corresponding to image (D). The spectrum reveals characteristic peaks from Te, confirming that the needles are made of single Te crystals, with residues from the organic content in the solutions providing EDX signal for P, S and Cl.

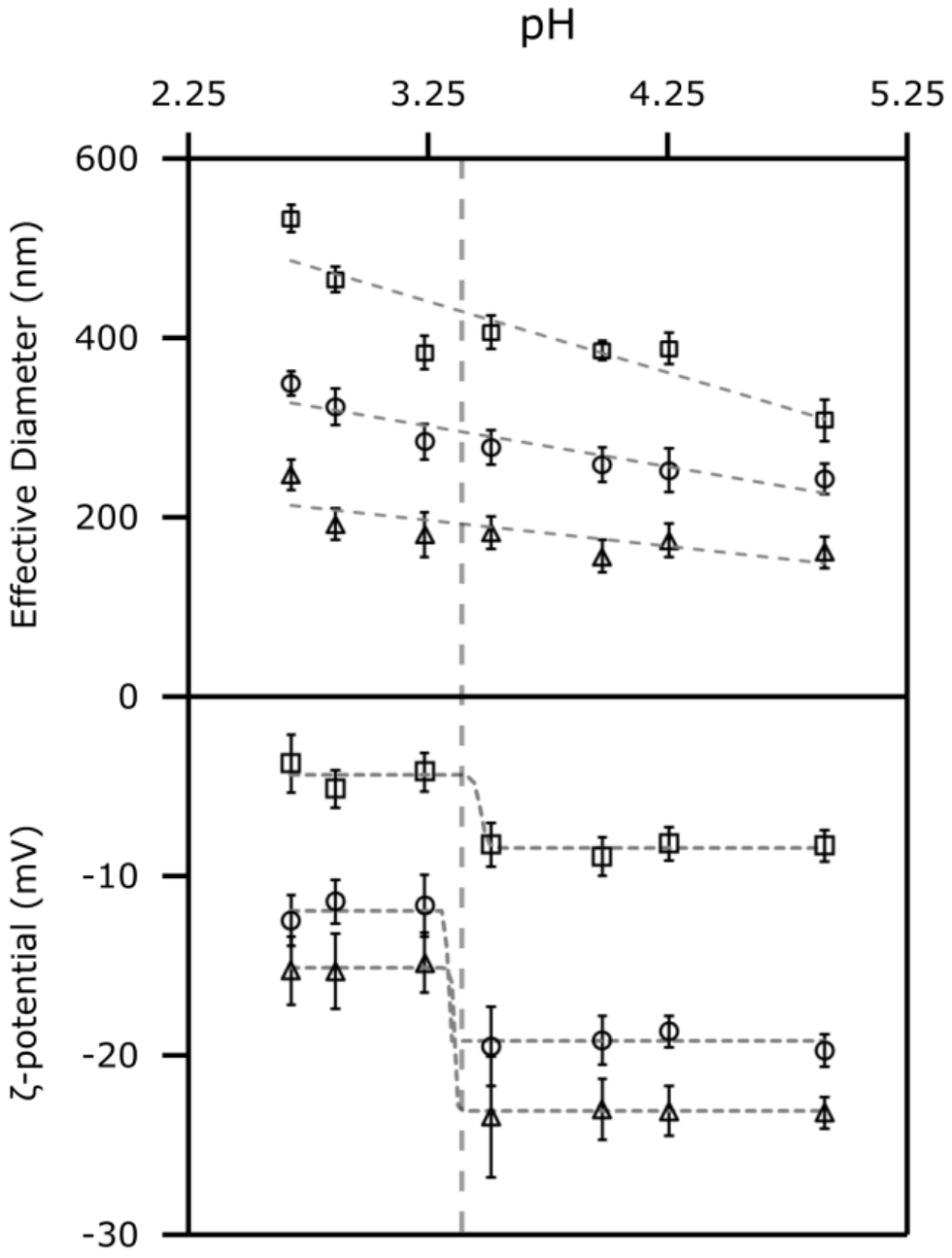

Figure 2. DLS and Zeta potential. Effective hydrodynamic diameter as measured via DLS (top) and zeta potential (ζ) values as measured via phase analysis light scattering (bottom) of NPs from three distinct production batches (circles, squares and triangles) at pH values ranging from 2.6 to 5.0. Error bars are the standard deviations of triplicate measurements performed on the same batch. Dashed gray curves in the ζ are Boltzmann sigmoidal fits of each batch. The vertical dashed line marks the average point of maximum slope of the sigmoid fits, which occurs at pH 3.45±0.05.

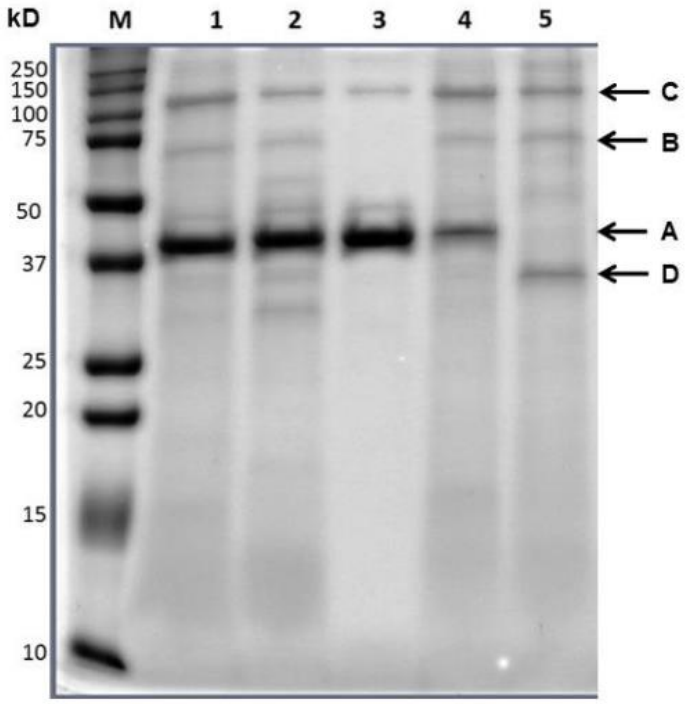

Figure 3. SDS-PAGE analysis of proteins solubilized from TeNPs. Lane 1, B100 (wt), tellurite 1 mM, lawsone 25 µM; lane 2, B100 tellurite 1 mM, lawsone 2 µM; lane 3, B100, no tellurite, lawsone 25 µM; lane 4, B100, tellurite 1 mM, lawsone 25 µM with an additional washing; lane 5, bKSDF (Δ*flaA*). Tellurite 1 mM, lawsone 25 µM. Bands A, B, C and D were excised and analyzed by LC-MS/MS.

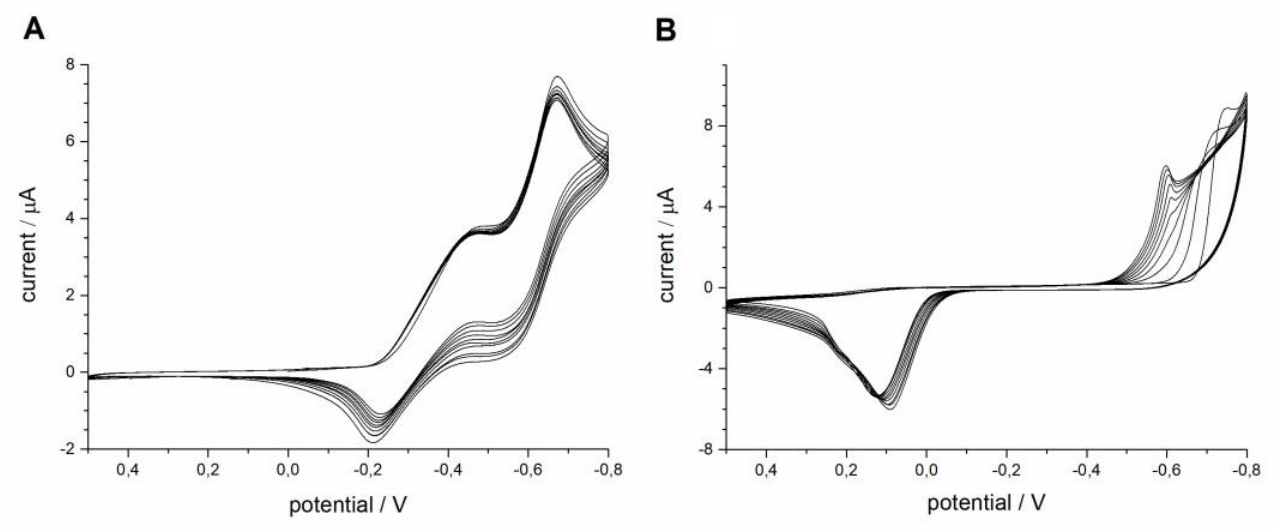

Figure 4. Cyclic voltammetry. (A) 5 mM lawsone. (B) 10 mM potassium tellurite. Cyclic voltammetry was performed at a scan rate of 0.02 V/s in PBS buffer in the absence of oxygen

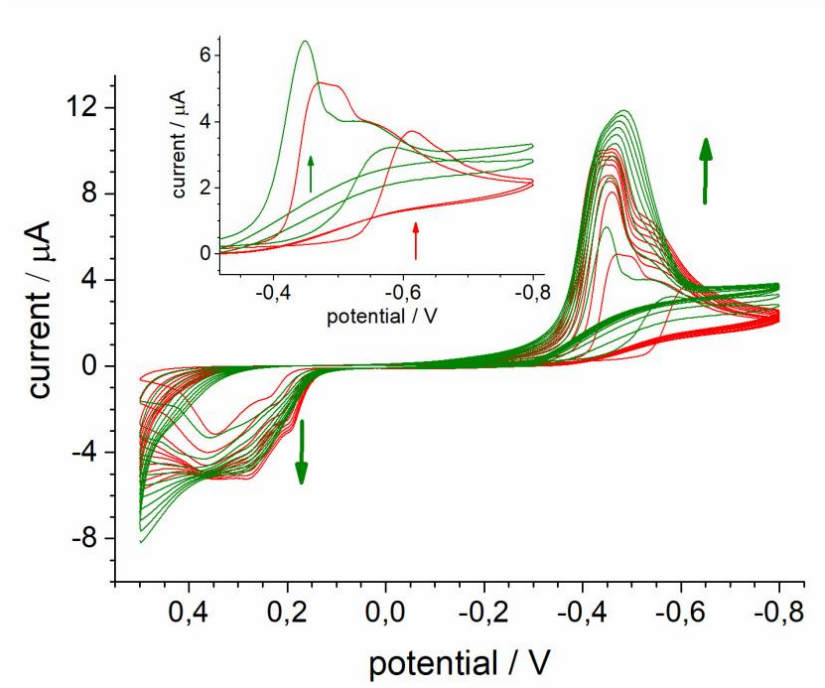

Figure 5. Cyclic voltammetry of 1 mM potassium tellurite in the presence of 25 µM lawsone (scan rate 0.02 V/s.). Red and green traces were obtained in the absence and in the presence of 25 µM lawsone, respectively. The arrows indicate the progressive change of peak intensities during cycling. The inset shows a magnification between -0.3 and -0.8 V of the first 3 cycles.

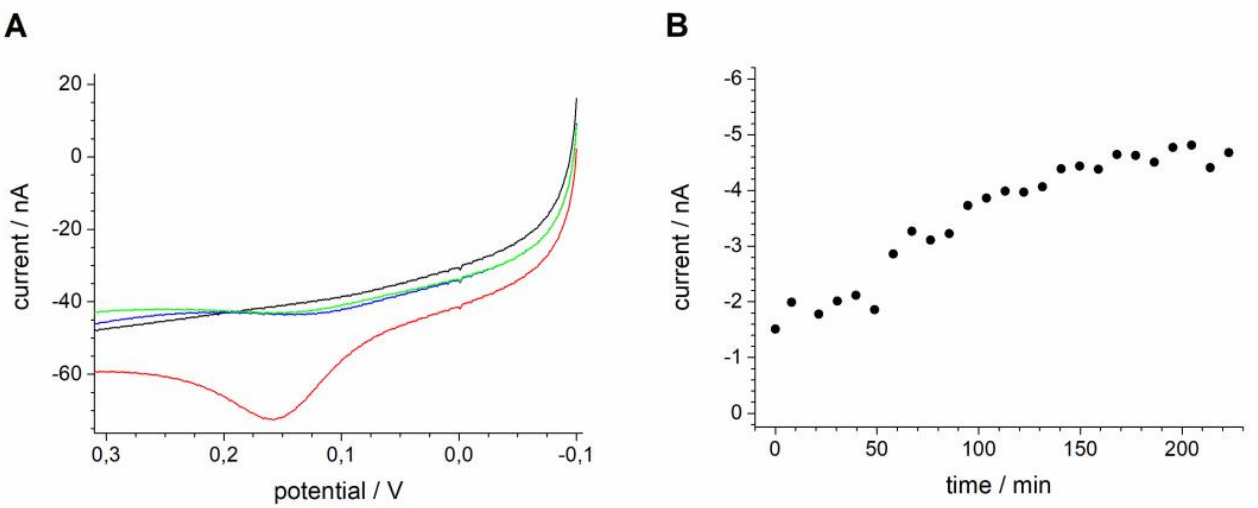

Figure 6. Electrochemical detection of tellurite reduction in the presence of bacteria, tellurite and lawsone in anaerobic light-culturing conditions. (A**)** Representative CVs with a scan rate of 0.02 V/s and scan range -0.1 and 0.4 V vs Ag/AgCl at 0 h (black), 2 h (green), 2.5 h (blue) and 5 h (red) after starting photosynthetic anaerobic cultures. (B) Time course of oxidation currents measured between 0.10-0.15 V vs Ag/AgCl during the first 250 minutes of cultures.

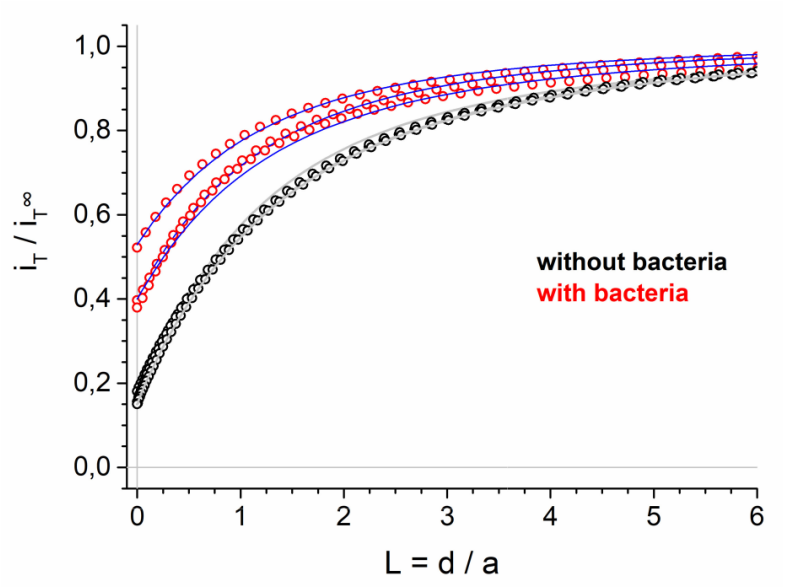

Figure 7. SECM approach curves. The approach curves experiments were done in the presence of 200 µM lawsone on a layer of bacteria attached with polylisine to the glass bottom of a petri dish. Normalized currents (I_T/I_∞) measured at the working electrode at -0.5 V vs Ag/AgCl as a function of L, the distance d of the probe extremity to the approached surface normalized to the tip radium a. Currents measured at the working microelectrode (I_T) were normalized to that measured in the bulk (I_∞). Black and red dots represent SECM approach curves obtained in the absence or in the presence of bacteria, respectively. Continuous lines are the best fit to theoretical models as reported in the main text.

Supplementary Information

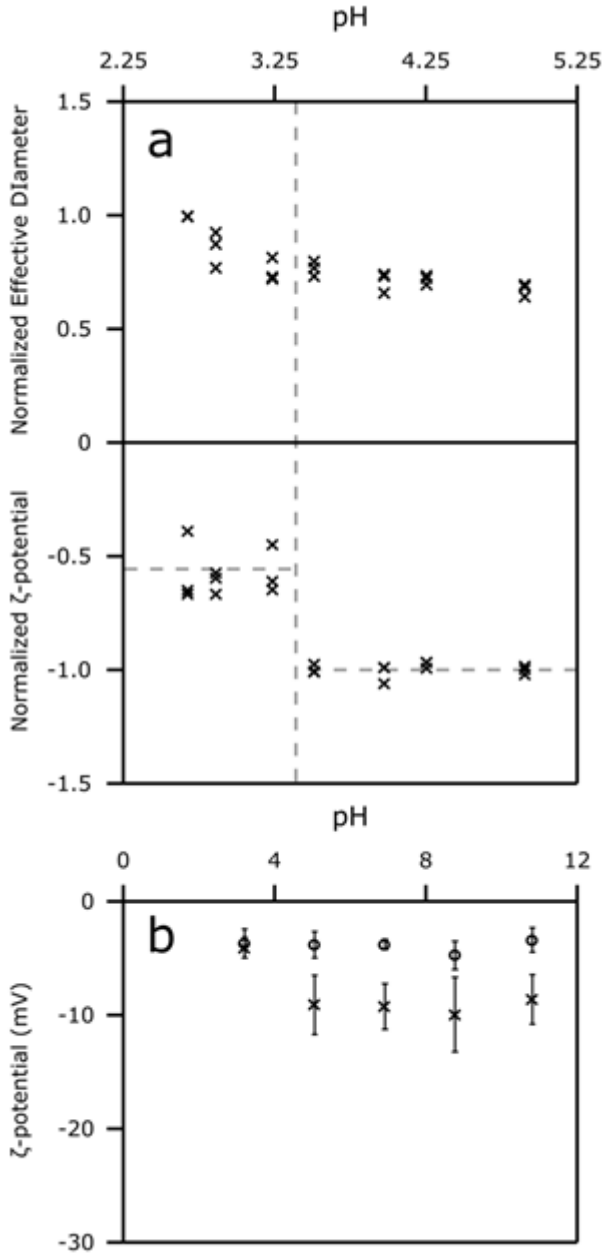

Figure S1. Zeta analysis (a): normalized plots of the same measurements shown in main text, Figure 2. Horizontal gray dashed lines in the ζ plot mark the average normalized zeta potential (ζ_N) values of all samples at pH values below 3.45 (avg. ζ_N = -0.55) or above it (ζ_N = -1.00). (b): proof of the pH reversibility of the induced ζ changes across all pH values. Circles denote individual samples (from the batch marked with squares in main text Figure 2), all suspended at pH 3.00: in this case, the plotted pH value is the pH at which they were suspended in the original batch. All samples at pH 3.00 show the same ζ value. Crosses are the same samples suspended at various pH values, which are close to those originally plotted in Figure 2.

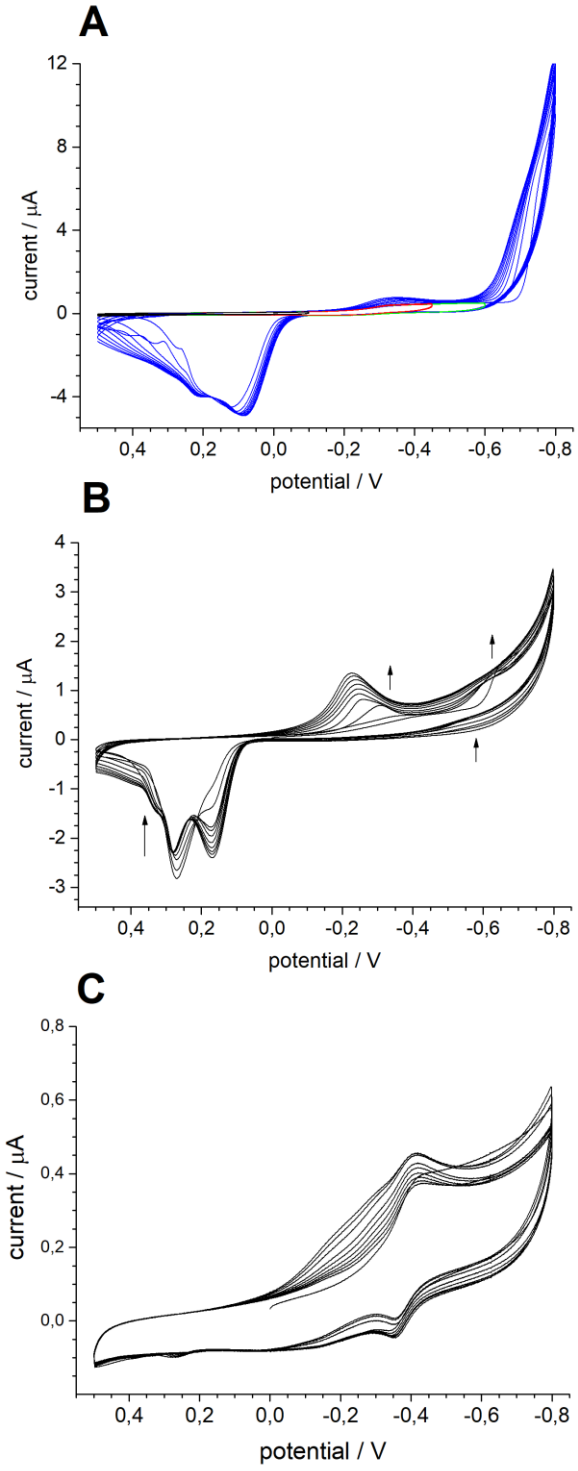

Figure S2. Characterization in the absence of oxygen of the electrochemical behaviour in the -0.8 ÷ 0.5 V range of tellurite and 25 µM lawsone in PBS buffer. The arrows indicate the change of peak intensities during cycling. (**A)** 10 mM potassium tellurite in PBS buffer; lower vertex potential was changed (-0.1, -0.4, -0.6 and -0.8 V for black, red, green and blue trace respectively). (**B)** 1 mM potassium-tellurite in PBS buffer. **(C)** 25 µM lawsone in PBS.

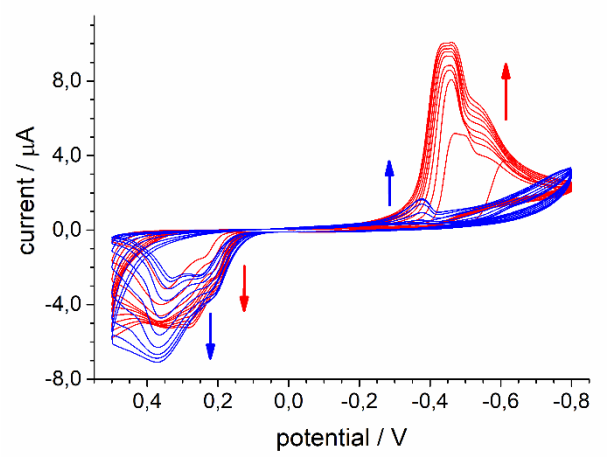

Figure S3. Cyclic voltammetries of 1 mM potassium-tellurite in PBS (blue) and RCV (red) medium. The arrows indicate the change of peak intensities during cycling.

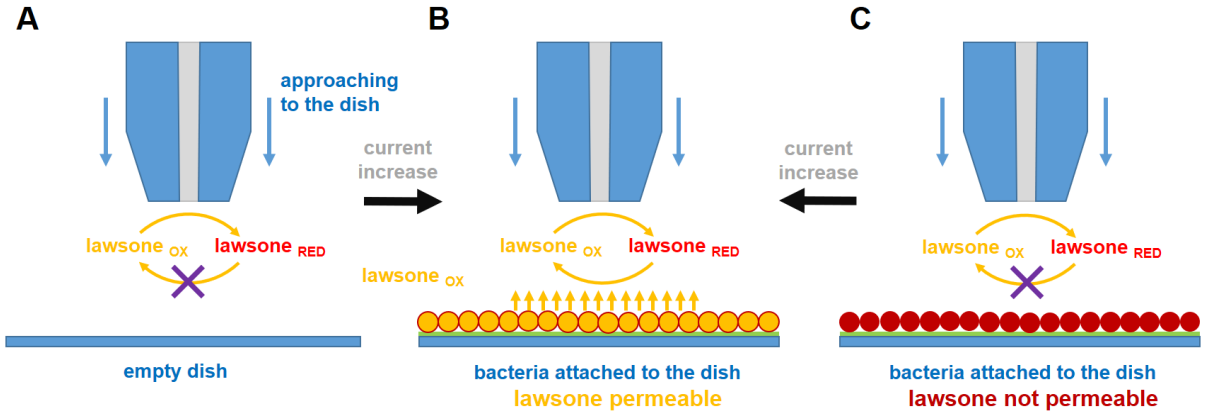

Figure S4. Scheme of SECM measurement of the lawsone diffusion inside bacteria. For an impermeable surface, **A** and **C** (i.e. empty dish or no diffusion of lawsone inside bacteria), the current decreases as the electrode approaches the surface because of the hindering diffusion. On the contrary, if the surface is permeable to the compound, **B** (i.e. if lawsone diffuses inside bacteria), diffusion of the compound from the permeable surface to the microelectrode probe reduces the effects of the hindered diffusion; as a result, if the surface has a permeability grade for the redox mediator (the lawsone in the present case), at the same distance from the surface of the probe higher currents has to be measured when compared to the impermeable surface.

Quantitative analysis of SECM approach curves.

Table 1

With bacteria		Without bacteria	
k	k_{eff} (cm s^{-1})	***k***	k_{eff} (cm s^{-1})
$2.18 \cdot 10^{-2}$	$3.09 \cdot 10^{-4}$	0	0
$1.62 \cdot 10^{-2}$	$2.30 \cdot 10^{-4}$	0	0
$4.96 \cdot 10^{-3}$	$0.7 \cdot 10^{-4}$	0	0

The dimensionless rate constant *k* was obtained by fitting SECM approach curves with MIRA software (Wittstock et al., 2000). Current-distance approach curves in the absence or in the presence of bacteria were fitted to equations describing purely negative feedback curves, i.e. insulating surface (Cornut et al., 2007), or finite reactions taking place at the approached surface (Cornut et al., 2008; Wittstock et al., 2007). For the finite reaction model, an effective first-order heterogenous constant $k_{eff} = (kD)/a$ (where *D* is the diffusion coefficient of the redox mediator, i.e. lawsone, and *a* is the radius of the electrode disk) can be calculated from *k* values. It has been showed (Koley et al., 2010) by SECM approach curves on Hela cells and COMSOL simulations, that k_{eff} returns valuable information on the diffusion of the redox mediator to cell interiors; in fact, permeability of redox mediators to cell membranes can be derived from k_{eff}.

For empty Petri dishes, best fits of SECM approaches were obtained with a model describing an insulating surface; finite reaction model returned worst results, as suggest from *k* values equal to 0. For Petri dishes with attached bacteria finite reaction model always returned best fits when compared to the pure insulating model; Table 1 shows *k* values obtained for the best fits and k_{eff} calculated considering $D \sim 7.1 \cdot 10^{-6}$ $cm^2\ s^{-1}$ for 1,4-naphtoquinone in water and $a = 5 \cdot 10^{-4}$ cm. k_{eff} values calculated in the presence of bacteria are in good agreement to those reported by Cai and colleagues (Cai et al., 2002) for 1,2-naphtoquinone and 1,4-naphtoquinone with *Rhodobacter sphaeroides*.

References

Cai, C., Liu, B., Mirkin, M.V. (2002). Scanning Electrochemical Microscopy of Living Cells. 3. *Rhodobacter sphaeroides*. *Anal. Chem.* 74, 114-119.

Cornut, R., and Lefrou, C. (2007). A unified new analytical approximation for negative feedback currents with a microdisk SECM tip. *J. Electroanal. Chem.* 608, 59–66. doi: 10.1016/j.jelechem.2007.05.007

Cornut, R., and Lefrou, C. (2008). New analytical approximation of feedback approach curves with a microdisk SECM tip and irreversible kinetic reaction at the substrate. *J. Electroanal. Chem.* 621, 178–184. doi: 10.1016/j.jelechem.2007.09.021

Koley, D., Bard, A.J. (2010). Triton X-100 concentration effects on membrane permeability of a single HeLa cell by scanning electrochemical microscopy (SECM). *P. Natl. Acad. Sci.* USA, 107, 16783-16787.

Wittstock, G., T. Asmus, T. Wilhelm, T. (2000). Investigation of ion-bombarded conducting polymer films by scanning electrochemical microscopy (SECM). Fresenius J. Anal. Chem. *2000*, 367, 346-351.

Wittstock, G., Burchardt, M., Pust, S.E., Shen, Y., Zhao, C. (2007). Scanning Electrochemical Microscopy for Direct Imaging of Reaction Rates. *Angew. Chem. Int. Ed*., 46, 1584-1617.